




# Microstructural characterization of rapidly solidified Al-13.5 at.% Cr and Al-13.5 at.% V alloys for catalytic applications

Amelia Zięba<sup>1</sup>, Katarzyna Stan-Głowińska<sup>1</sup>, Łukasz Rogal<sup>1</sup>, Paweł Czaja<sup>1</sup>, Janusz Przewoźnik<sup>2</sup>, Robert Chulist<sup>1</sup>, Dorota Duraczyńska<sup>3</sup>, and Lidia Lityńska-Dobrzyńska<sup>1,\*</sup> 

<sup>1</sup> The Aleksander Krupkowski Institute of Metallurgy and Materials Science, Polish Academy of Sciences, Reymonta 25, 30-059 Krakow, Poland

<sup>2</sup> Faculty of Physics and Applied Computer Science, Department of Solid State Physics, AGH University of Science and Technology, Al. Mickiewicza 30, 30-059 Krakow, Poland

<sup>3</sup> The Jerzy Haber Institute of Catalysis and Surface Chemistry, Polish Academy of Sciences, Niezapominajek 8, 30-239 Krakow, Poland

**Received:** 13 February 2023

**Accepted:** 7 August 2023

**Published online:**  
29 August 2023

© The Author(s), 2023

## ABSTRACT

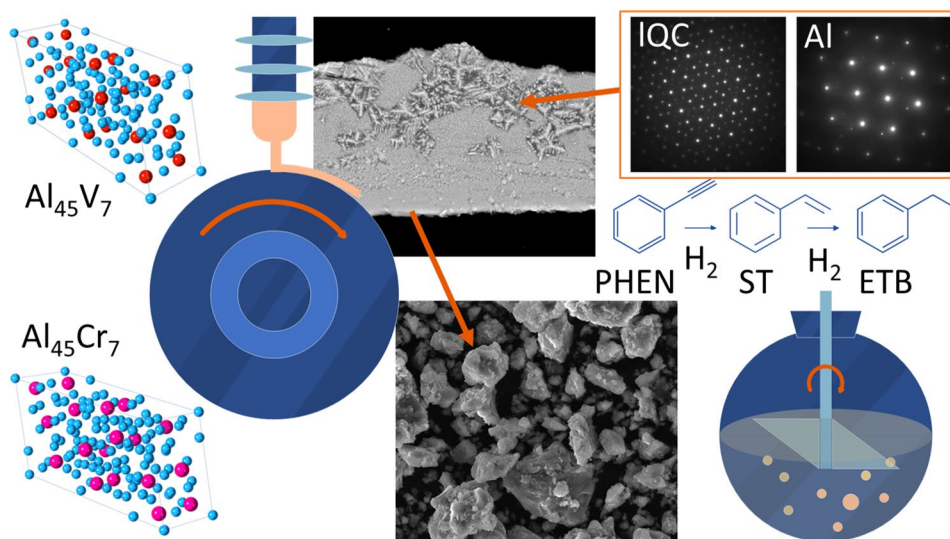
Intermetallic compounds, due to their well-defined stoichiometry, arrangement of atoms and controlled crystal structure, are a promising alternative to expensive noble metal catalysts. In this paper, the catalytic properties of Al-13.5 at.% Cr and Al-13.5 at.% V alloys, corresponding to the quasicrystalline approximants  $Al_{45}Cr_7$  and  $Al_{45}V_7$ , were investigated for the first time.

The alloys in the form of fragmented brittle ribbons were produced by the melt-spinning. The microstructure of the ribbons, both in the as-spun state and after heat treatment (100 h at 600 °C), was characterized by X-ray diffraction, scanning electron microscopy and transmission electron microscopy. In the as-spun state, the ribbons showed a multiphase microstructure. In addition to the  $Al_{45}Cr_7$  phase in the Al-Cr alloy and the  $Al_3V$  phase in the Al-V alloy, they also contained  $\alpha(Al)$  solid solution and icosahedral quasicrystalline phases. After heat treatment, the alloys became almost single phase, consisting mainly of stable monoclinic phases:  $Al_{45}Cr_7$  or  $Al_{45}V_7$ . The catalytic performance of the phenylacetylene hydrogenation reaction was tested on as-spun and heat-treated alloys that had previously been pulverized and sieved to select a powder fraction of less than 32  $\mu m$ . All the tested materials show high substrate conversion, above 80% after 1 h reaction, along with high activity rate. The homogenized powders demonstrated a slightly better properties in relation to as-spun materials. These results confirm the potential of intermetallic catalysts, including the tested alloys, in hydrogenation reactions and verify the possibility of using the metallurgical method to obtain catalytically active materials.

Handling Editor: Yaroslava Yingling.

Address correspondence to E-mail: l.litynska@imim.pl

## GRAPHICAL ABSTRACT



## Introduction

In recent years, the idea of the application of intermetallic compounds in catalytic processes has been increasingly considered [1–6]. Theoretical studies have shown the crucial role of a well-defined structure and chemical composition of the catalyst, which leads to the formation of electronic structures enabling interaction with reactant particles and the desired reaction paths [7–11]. Promising results of experiments on palladium-based intermetallics encouraged the search for new groups of compounds, also based on non-noble metals [e.g. 12–16]. The development of these solutions can be a prospect for a wide range of chemical industry applications as an environmentally friendly, low-cost alternative. Additionally, the fact that many of the proposed intermetallic catalysts are effective under mild reaction conditions, resulting in low-energy consumption, encourages further research in this field.

In particular, aluminium-based intermetallic compounds containing transition metals showed excellent properties due to their crystallographic structure and electronic properties. So far, the conducted research has focused mainly on compounds containing Fe or Co as active metals, including structures related to quasicrystalline phases [17–21]. The fact that chromium and vanadium in various forms were successfully used as catalysts in a wide spectrum of reactions in organic chemistry [22–25] was the reason for undertaking

studies of intermetallic phases from Al–Cr and Al–V systems.

Two intermetallic phases  $\text{Al}_{45}\text{Cr}_7$  and  $\text{Al}_{45}\text{V}_7$ , which are quasicrystal approximants, were selected for the research in this work. The  $\text{Al}_{45}\text{Cr}_7$  phase, previously known as  $\text{Al}_7\text{Cr}$ , is in the range of 12.5–14 at.% in the aluminium-rich region of the Al–Cr phase diagram [26].  $\text{Al}_{45}\text{Cr}_7$  is a complex intermetallic compound containing 104 atoms in a monoclinic unit cell (C2/m space group) with the lattice parameters ( $a = 2.0595$  nm,  $b = 0.75974$  nm,  $c = 1.0949$  nm and  $\beta = 107.34^\circ$ ) [27, 28]. This phase is an approximant of an icosahedral quasicrystal that can be formed during the rapid solidification process [29]. The  $\text{Al}_{45}\text{V}_7$  phase, isostructural to the  $\text{Al}_{45}\text{Cr}_7$  phase, has a very narrow homogeneity range and occurs at the content of 13.5 at.% of V [30]. The structure of this phase has not been widely described, but the available sources indicate a monoclinic cell (C2/m space group) with lattice constants  $a = 0.2560$  nm,  $b = 0.7621$  nm,  $c = 1.108$  nm and  $\beta = 128.55^\circ$  [31]. Under non-equilibrium conditions, an icosahedral quasicrystal may also form in the alloy with the chemical composition referring to the  $\text{Al}_{45}\text{V}_7$  phase, produced by rapid solidification techniques [32, 33].

The aim of this work was to verify (to our knowledge for the first time) the use of two intermetallic alloys with a chemical composition corresponding to the  $\text{Al}_{45}\text{Cr}_7$  and  $\text{Al}_{45}\text{V}_7$  phases as catalysts. For this purpose, the hydrogenation of phenylacetylene was

chosen as the reaction to produce styrene, which is a widely used substrate in the petrochemical industry. The current approach for the synthesis of styrene requires development due to the expensive and scarce palladium-based catalysts that also get poisoned, which drastically reduces the selectivity of the catalyst [34]. Therefore, extensive work is being carried out on alternatives that do not contain noble metals or eliminating expensive components. In addition, phenylacetylene hydrogenation reaction was conducted with other intermetallic compounds under the same conditions, which allows for a direct comparison of the results obtained. The investigated alloys were produced by the melt-spinning method and additionally subjected to homogenization heat treatment. The choice of the alloy preparation method was due to the promising results obtained previously for  $\text{Al}_{13}\text{X}_4$  and  $\text{Al}_5\text{X}_2$  ( $\text{X} = \text{Fe}, \text{Co}$ ) ribbons [19, 20], which enabled relatively easy obtaining of the catalyst in the form of powder. The phase composition and microstructure of proposed materials were examined by X-ray diffraction, scanning and transmission electron microscopy. The powdered as-spun and annealed ribbons were used as a catalyst for the reaction taking place in the liquid medium, and their catalytic activity was evaluated.

## Materials and methods

### Materials

The alloys with nominal compositions Al-13.5 at.% Cr and Al-13.5 at.% V (designated as Al-13.5Cr and Al-13.5 V, respectively) were cast in an induction furnace under an argon atmosphere using high-purity elements (99.99%). The ingot pieces were re-melted in the quartz crucible with a bottom hole of 0.8 mm in diameter and cast by melt-spinning technique. Melting and casting were performed in a protective helium atmosphere. The liquid alloy was ejected onto a surface of a copper wheel rotating at a linear speed of 20 m/s. The pressure of the gas ejecting the molten alloy was 0.180 MPa. The obtained alloys were in the form of fragmented brittle ribbon flakes. Half of the ribbons from both materials were encapsulated in a quartz ampule under vacuum, heat-treated at 600 °C for 100 h and then quenched in water. Prior to the catalytic tests, the as-spun and annealed ribbons were pulverized using a vibration micro-mill PULVERISETTE 0 with tungsten

carbide mortar and grinding ball (50 mm in diameter). The time of milling was 30 min. The obtained powders were sieved by vibratory sieve shaker Fritsch Analysette 3 to select the powder fraction below 32  $\mu\text{m}$ .

### Microstructural characterization

Microstructural observations, chemical analysis and crystallographic characterizations of the samples were performed using a combination of X-ray diffraction, scanning electron microscopy (SEM) and transmission electron microscopy (TEM).

Phase compositions of the pulverized ribbons were examined by X-ray diffraction using a Panalytical Empyrean diffractometer and an X'Celerator linear detector with  $\text{Cu-K}\alpha$  radiation ( $\lambda = 0.1540598 \text{ nm}$ ), and a rear graphite monochromator. The obtained data were analysed using the profile fitting programme FullProf [35] and a profile matching method. The background intensity was approximated with a polynomial function, and the peak shape was adjusted by a pseudo-Voigt function. The as-spun ribbons were examined by synchrotron SR-XRD technique using high-energy X-ray diffraction measurements at DESY in Germany, Hamburg, with beamline P07B (87.1 keV,  $\lambda = 0.0142342 \text{ nm}$ ). For phase analysis, diffraction patterns were recorded in the so-called continuous mode using a 2D Mar345 Image Plate detector. The samples were rotated 180° around the  $\omega$ -axis when X-rayed to obtain texture-less measurements [36].

The as-spun ribbons as well as the pulverized ribbons were investigated using FEI-SEM XL30 scanning microscope equipped with EDAX Genesis EDS spectrometer. Standard analyses were carried out at accelerating voltages of 20 kV and a working distance of 8 mm. In order to obtain a compositional contrast between the different phases in the sample, the back-scattered electron signal (BSE mode) was selected. To analyse the longitudinal cross-section of the ribbons, their fragments were embedded in epoxy resin, grinded with SiC paper and then polished with diamond paste. The powder samples in as-spun and heat-treated states were applied to adhesive tape to examine their external morphology and determine the particle size.

Detailed microstructural studies were provided by FEI Tecnai G2 FEG super TWIN transmission electron microscope operating at 200 keV and equipped with a high-angle annular dark field scanning

transmission electron microscopy detector (HAADF-STEM) combined with energy-dispersive X-ray (EDX) EDAX microanalysis. Elemental composition measurements were performed by energy-dispersive X-ray spectroscopy (EDS) in STEM mode using camera length of 200 mm, appropriate for Z-contrast HAADF imaging. The crystal structure of the phases was analysed by selected area electron diffraction method. Thin foils for TEM were prepared from the ribbons by punching discs with a diameter of 3 mm and electropolishing by Tenupol-5 double jet at  $-30\text{ }^{\circ}\text{C}$  and 12 V using an electrolyte of nitric acid and methanol (1:2 vol.) to obtain perforations.

### Hydrogenation experiments

The catalytic activity of the powdered as-spun and annealed ribbons was tested in the semi-hydrogenation of phenylacetylene to styrene with 2-propanol as a solvent. Before the catalytic tests, the surface of the powders was treated with an aqueous  $\text{NaBH}_4$  solution to remove possible oxidation. The reduced powder, reagent and solvent placed in an agitated batch glass reactor were continuously stirred during the tests. The composition of the reaction mixtures was characterized using a gas chromatograph (Clarus 500, Perkin Elmer) with He as carrier gas (flow rate 1 ml/min). Styrene and ethylbenzene were the only observed products. The content of reactants was determined by comparison with the calibration curves. No reaction was observed in a blank run in the absence of catalyst or hydrogen flow.

## Results and discussion

### Al-13.5Cr ribbon

The observation of the longitudinal cross-section of the Al-13.5Cr ribbon by the scanning electron microscope backscattered electrons (SEM-BSE) method revealed a non-uniform microstructure both in length and thickness. The thickness of the ribbon was found to vary in the range of 20–70  $\mu\text{m}$  (Fig. 1) along its length. The lower edge of the ribbon is smooth, indicating that it has solidified on the surface of the copper wheel (wheel side), while the upper roughened edge has been in contact with the helium atmosphere (free side). The thick ribbon shown in Fig. 1a contains two regions: an almost featureless region with single dendrites at the wheel side and a dendritic microstructure near the free side. Reducing the thickness of the ribbon leads to the disappearance of the dendrite zone. Almost in the entire volume of the ribbon, a homogeneous structure is visible, with rarely occurring columnar grains growing from the wheel side (Fig. 1b and c). The formation of different microstructure variants results from local conditions during the melt-spinning and the progressive reduction of the cooling rate from the wheel to the free side. Similar microstructures were observed in Al-Mn-Be [37], Al-Mn-Fe [38] and Al-Mn [39]; hence, the presented microstructure seems to be typical for rapidly solidified aluminium-based ribbons.

Three phases have been identified in the Al-13.5Cr ribbon based on the synchrotron X-ray diffraction pattern: the  $\text{Al}_{45}\text{Cr}_7$  phase, the icosahedral quasicrystal and the  $\alpha(\text{Al})$  solid solution (Fig. 2a). The main phase

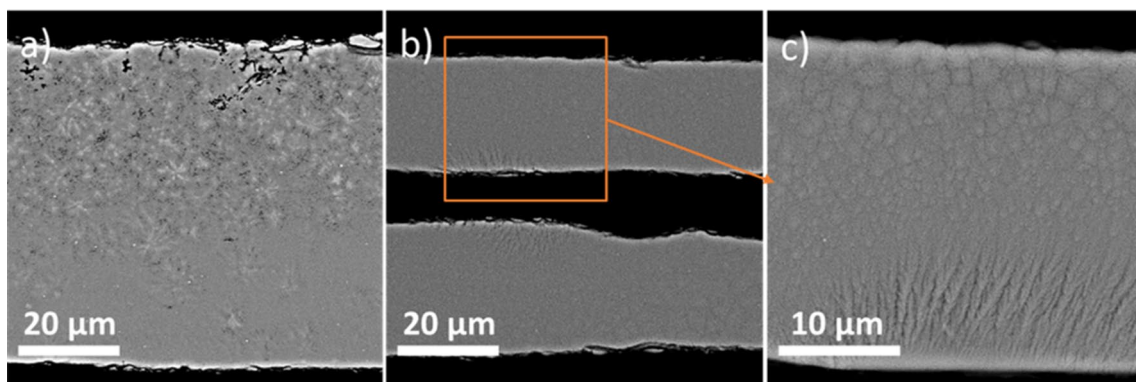


**Figure 1** SEM-BSE micrographs of a longitudinal cross-section of the as-spun Al-13.5Cr ribbon of different thicknesses **a** about 70  $\mu\text{m}$  and **b**, **c** about 30  $\mu\text{m}$



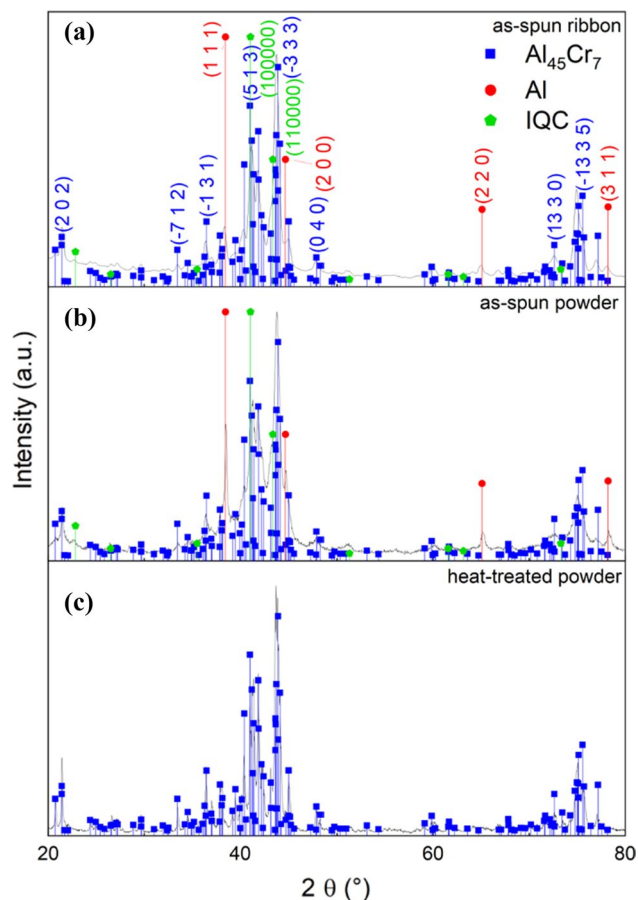


**Figure 2** X-ray patterns of the Al-13.5Cr ribbon in the as-spun state **a**, as-spun ribbon after pulverization **b** and after annealing 100 h/600 °C **c**

with a mass fraction of about 84% is the  $\text{Al}_{45}\text{Cr}_7$  intermetallic compound, which is between 12.5 and 14 at.% of Cr in the phase diagram presented by Okamoto [26]. The monoclinic  $\text{Al}_{45}\text{Cr}_7$  (C2/m) phase with lattice constants  $a = 2.0595$  nm,  $b = 0.7574$  nm,  $c = 1.0949$  nm and  $\beta = 107.34^\circ$  composed of icosahedral clusters is an approximant of icosahedral quasicrystal [27, 40]. The presented X-ray pattern shows the first characteristic reflection of the icosahedral quasicrystal at the position of  $22.8^\circ$  [41], while the remaining quasicrystalline peaks overlap with the reflections of the  $\text{Al}_{45}\text{Cr}_7$  phase. The estimated mass fraction of the quasicrystal was about 7.2%. Additional reflections in the X-ray plot are attributed to the  $\alpha(\text{Al})$  solid solution. Contrary to our results, the icosahedral phase reported previously in the rapidly solidified ribbons containing Cr in the range from 4 to 15 at.% was usually dominant compared to the other phases [42–45]. The difficulty in forming the icosahedral phase in our case may be due

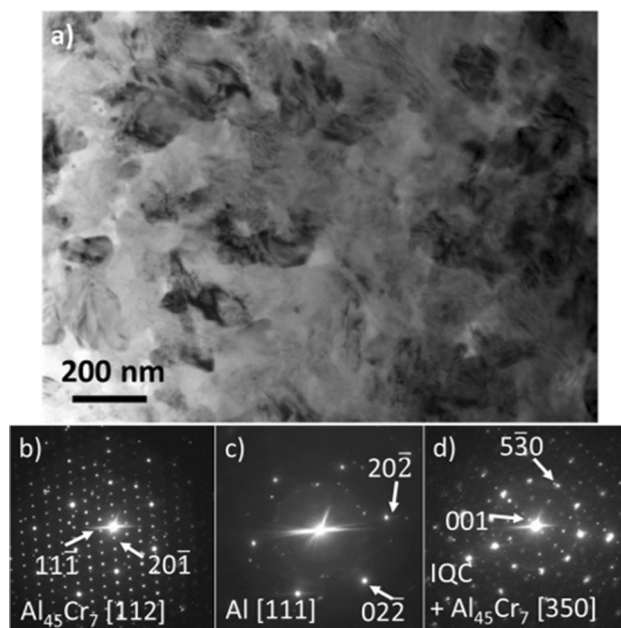


**Figure 3** Al-13.5Cr ribbon: **a** TEM bright-field image and SADPs of **b** the  $\text{Al}_{45}\text{Cr}_7$  phase along [112] zone axis **c**  $\alpha(\text{Al})$  solid solution along [111] zone axis and **d** icosahedral quasicrystal with fivefold symmetry and  $\text{Al}_{45}\text{Cr}_7$  along [350] zone axis

to the fact that the cooling rate of the melt-spinning apparatus is not high enough to suppress the formation of a stable  $\text{Al}_{45}\text{Cr}_7$  intermetallic compound.

The microstructure of the as-spun Al-13.5Cr ribbon registered using TEM contains a mixture of fine grains about 200 nm in size with the structure of internal defects (Fig. 3a). The EDX point microanalysis showed differences in the chemical composition of the grains; some grains contained about 98 at.% of Al and 2 at.% of Cr, others were enriched in Cr (12 at.% of Cr and 88 at.% of Al). The SADP obtained for individual grains allowed for the identification of the same phases, which can be seen in the X-ray diffraction pattern (Fig. 2a). The Cr-enriched grains were found to consist of the  $\text{Al}_{45}\text{Cr}_7$  phase or icosahedral quasicrystal. The SADP presented in Fig. 3b was described as the [112] zone axis of the  $\text{Al}_{45}\text{Cr}_7$  phase. Some of the observed SADPs contained the reflections corresponding to the icosahedral quasicrystal in addition to the reflections of the crystalline phase. Figure 3d shows an example of superimposed diffraction patterns of the  $\text{Al}_{45}\text{Cr}_7$  phase taken along the [350] zone axis and the fivefold symmetry of icosahedral quasicrystal. The bright areas between the grains were identified as  $\alpha(\text{Al})$  solid solution, and the corresponding SADP of  $\alpha(\text{Al})$  solid solution along the [111] zone axis is shown in Fig. 3c.

Prior to the catalytic tests, the as-spun and annealed Al-13.5Cr ribbons were pulverized by ball milling. Based on the literature reports, it has been found that the phase composition of the powdered ribbon can be significantly changed compared to the as-spun state due to internal strain and disorder introduced during milling. For example as the milling time progresses, the body-centred tetragonal crystal structure is transformed into a face-centred cubic in Ni–Mn–Ga melt-spun ribbons, which, in turn, leads to the suppression of the martensitic transformation and degradation of the magnetic moment [46, 47]. Therefore, the X-ray measurement of the pulverized as-spun ribbons was carried out in order to check the influence of the milling process on the phase composition (Fig. 2b). Comparing the X-ray diffraction patterns shown in Fig. 2a and b, it was found that both are almost identical. It follows that the short milling time (30 min) of the tested ribbons does not introduce any significant changes in their structure.

The morphology of the powdered as-spun Al-13.5Cr ribbon is shown in the SEM-BSE image in Fig. 4a and b. The powder particles have irregular shapes with sharp edges. Their sizes vary considerably, and much smaller particles can be seen between larger ones. The surfaces of large particles are not smooth and are covered with fine elements (Fig. 4b). The size distribution has been found to range from less than 1  $\mu\text{m}$  to 30  $\mu\text{m}$ . The estimated average size of the powder particles is 4.4  $\mu\text{m}$  (Fig. 4c). The powdered Al-13.5Cr ribbons annealed for 100 h at 600  $^{\circ}\text{C}$  are presented in Fig. 4d and e. Compared to the as-spun powder, the particle size appears to be slightly smaller. The estimated average dimension of powder particles is about 3.6  $\mu\text{m}$  (Fig. 4f). The larger particles do not have sharp edges in this case and look like agglomerates of smaller particles.

Annealing the Al-13.5Cr ribbon for 100 h at 600  $^{\circ}\text{C}$  promotes the formation of a single phase, as shown in the X-ray pattern (Fig. 2c). Reflections of the  $\alpha(\text{Al})$  solid solution disappeared, and only peaks of the

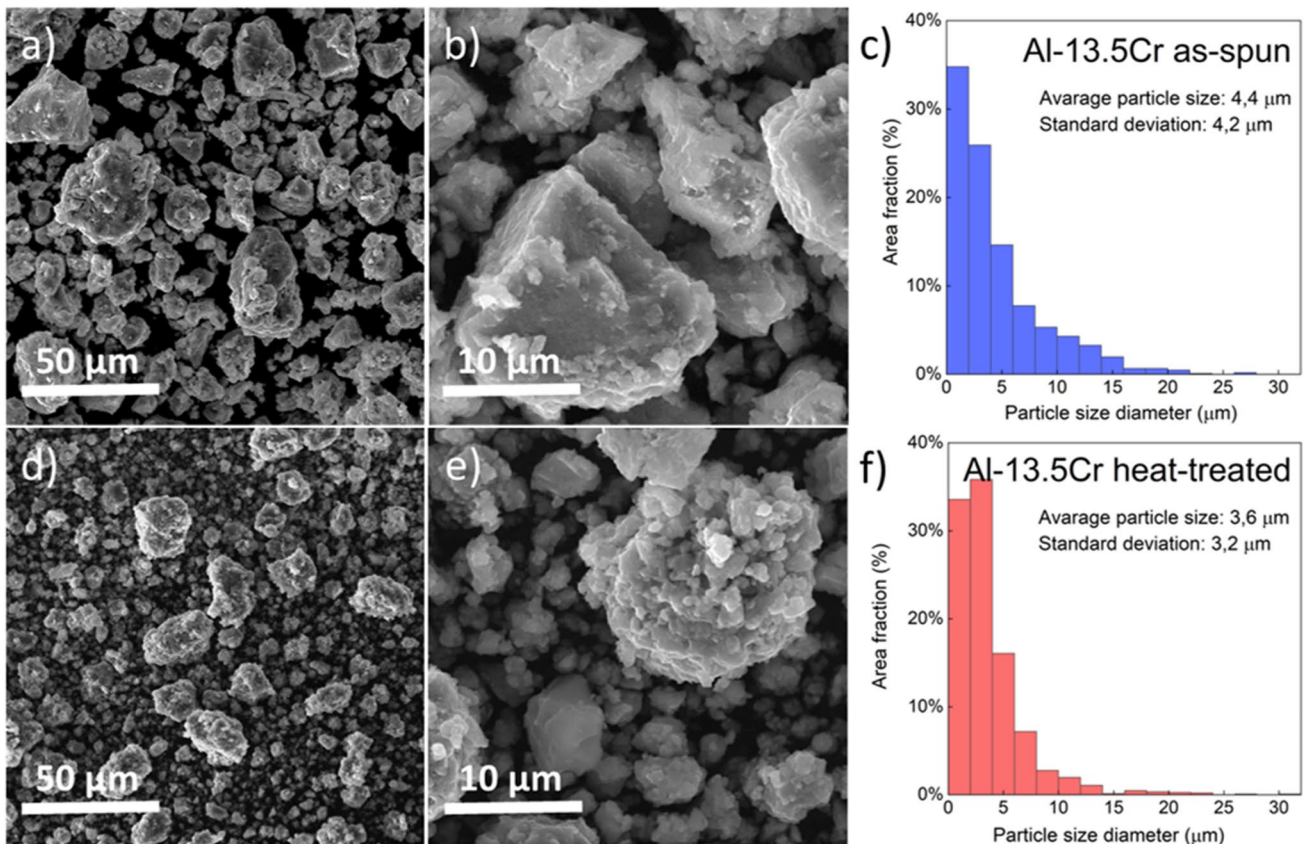


**Figure 4** SEM-BSE micrographs of the Al-13.5Cr ribbon after pulverization in the as-spun state **a, b** and annealed powdered ribbon **d, e**, corresponding histograms showing the particle size distribution are seen in **c, f**

stable  $\text{Al}_{45}\text{Cr}_7$  phase were identified. This result was confirmed by TEM observation of thin foils. It can be seen that the transformation to the single-phase microstructure was associated with grain growth compared to the as-spun state. Figure 5a shows an example of the TEM bright-field image containing grains with dimensions of the order of  $1\ \mu\text{m}$ . The morphology of the grains has also changed, and they have become smooth. The SADPs obtained from

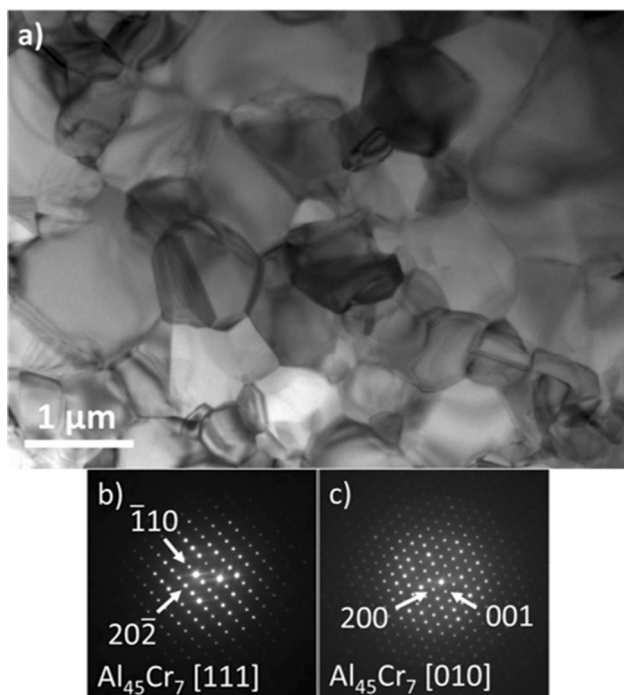


**Figure 5** a TEM bright-field image of the Al-13.5Cr ribbons after annealing for 100 h at  $600\ ^\circ\text{C}$  and b, c SADPs obtained for the separate grains of  $\text{Al}_{45}\text{Cr}_7$  phase

separate grains taken along the [010] and [111] zone axis are shown in Fig. 5b and c.

### Al-13.5 V ribbon

Figure 6 shows the longitudinal cross sections of the as-spun Al-13.5 V ribbon, showing changes in the microstructure along the length and distance from the cooling substrate, similar to the Al-13.5Cr as-spun ribbon. In the cross-section of a thick ribbon, two regions can be distinguished, homogeneous at the wheel side and dendrites on the free side (Fig. 6a), while the thin ribbon is nearly uniform throughout its volume (Fig. 6b). The enlarged SEM-BSE microstructure (Fig. 6c) showed that the homogeneous area is composed of fine spherical particles placed between rarely appearing dendrites.

The X-ray measurements allowed to identify three phases occurring in the as-spun Al-13.5 V ribbon: the  $\text{Al}_3\text{V}$  phase, the  $\alpha(\text{Al})$  solid solution and the icosahedral quasicrystal (Fig. 7a). The tetragonal  $\text{Al}_3\text{V}$  phase (space group  $I4/mmm$  and lattice constants  $a = 0.378\ \text{nm}$  and  $c = 0.8322\ \text{nm}$  [48]) is dominant together with  $\alpha(\text{Al})$  solid solution. The icosahedral phase coexisting with an aluminium solid solution and the tetragonal  $\text{Al}_3\text{V}$  phase in the rapidly solidified ribbon of similar composition (14.3 at% V) has been reported by Inoue et al. [49].

TEM studies provided detailed information on the microstructure of the as-spun ribbon. Two types of microstructure were found according to the SEM observations. Figure 8a shows the microstructure corresponding to the areas near the free side that contained small particles (up to  $0.5\ \mu\text{m}$ ) embedded in the  $\alpha(\text{Al})$  solid solution. The quasicrystalline phase was

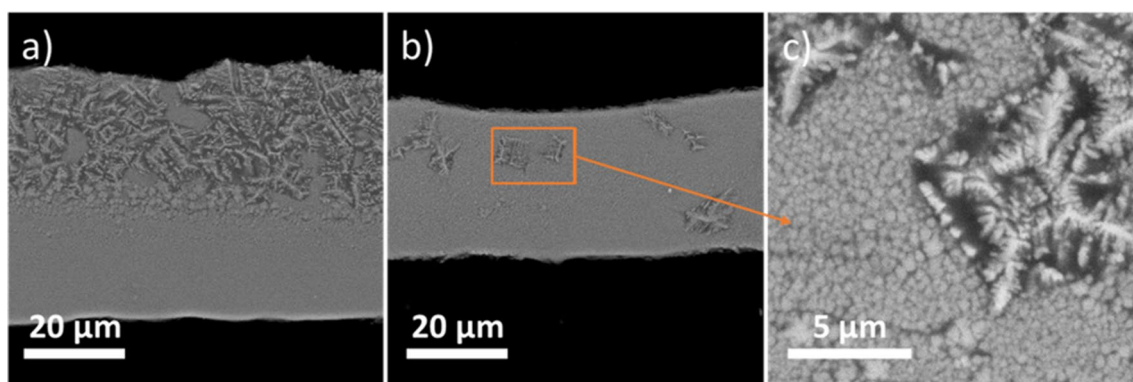


**Figure 6** SEM-BSE micrographs of the Al-13.5 V ribbon in the as-spun state



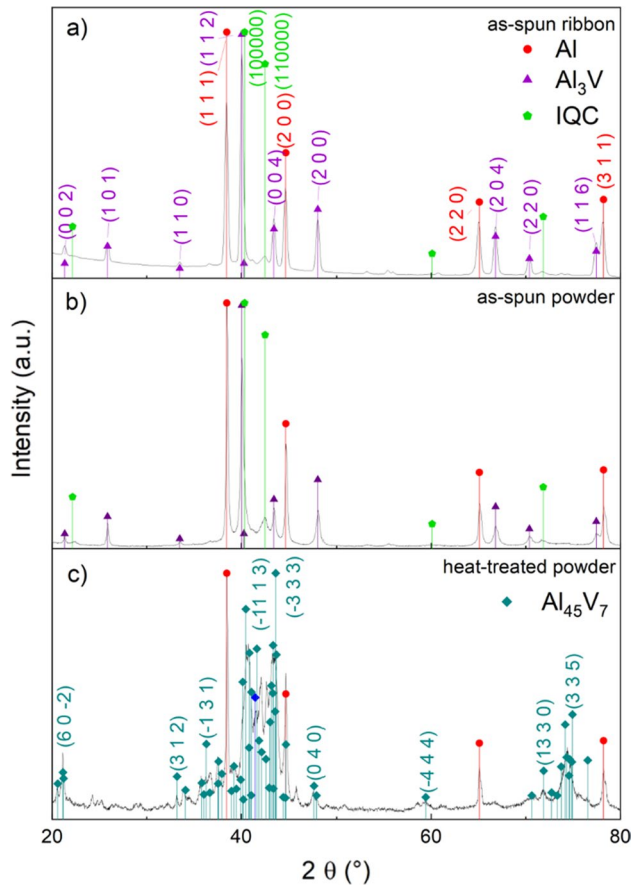


**Figure 7** XRD patterns of the Al-13.5 V ribbon in the as-spun state **a**, the as-spun ribbon after pulverization **b** and after heat treatment for 100 h at 600 °C

identified from the SADPs obtained for the single particles with five-, three- and two-fold symmetry typical for icosahedral quasicrystal (Fig. 8c–e). The SADP taken from the area between the quasicrystalline particles confirmed the  $\alpha(\text{Al})$  structure (Fig. 8f). The TEM bright-field image of the dendrite that formed near the free side of the ribbon is shown in Fig. 8b. The SADP corresponding to the visible dendrite was identified as the  $\text{Al}_3\text{V}$  phase (Fig. 8g), while the surrounding region as  $\alpha(\text{Al})$  solid solution (Fig. 8h).

The SEM-BSE micrographs of the pulverized ribbon obtained by milling the as-spun Al-13.5 V ribbon are presented in Fig. 9a and b. The average size of the powder particles was estimated to be about 5.4  $\mu\text{m}$  (Fig. 9c). The observed particles have sharp edges, and the smaller particles are partially agglomerated. It was found, as in the case of the powdered Al-13.5Cr ribbon, that the X-ray pattern (Fig. 7b) contained the reflections at the same positions as in the as-spun

ribbon (Fig. 7a). It can, therefore, be concluded that the milling process does not affect the phase composition of the alloy. The particles of the powdered heat-treated ribbon (100 h/600 °C) are finer in comparison with the as-spun powder (Fig. 9d and e), and their average size is 4.1  $\mu\text{m}$  (Fig. 9f). Annealed powders were also characterized by a larger agglomeration of small particles.

The X-ray of the annealed ribbon (Fig. 7c) showed two phases: the  $\text{Al}_{45}\text{V}_7$  phase (mass fraction about 90%) and the small amount of  $\alpha(\text{Al})$  solid solution (10%). It means that the metastable quasicrystalline phase and  $\text{Al}_3\text{V}$  transformed to the stable  $\text{Al}_{45}\text{V}_7$  phase, according to the phase diagram presented by Okamoto [30].

TEM bright-field image also contained a two-phase microstructure in the form of elongated grains visible in Fig. 10a. The SADPs obtained for both areas confirmed their structure:  $\text{Al}_{45}\text{V}_7$  (Fig. 10b) and  $\alpha(\text{Al})$  solid solution (Fig. 10c).

### Catalytic tests

The catalytic properties of manufactured alloys were evaluated for pulverized Al-13.5Cr and Al-13.5 V ribbons in an as-spun and annealed state with particle diameters below 32  $\mu\text{m}$ . However, as shown in Fig. 4 and Fig. 9, most of the powder particles were much smaller, and their estimated average dimensions were around 5  $\mu\text{m}$  for all tested materials. Experiments were performed with mild reaction parameters to ensure low-energy consumption and environmentally friendly conditions. Reactions were carried out under  $\text{H}_2$  pressure of 5 bar in a reactor heated to 50 °C by a water coat. Isopropanol was used as a solvent for phenylacetylene. In addition to styrene, ethylbenzene can be formed during the reaction as a result of the complete hydrogenation of the unsaturated carbon–carbon triple bond. The tracking of the reaction course was provided by composition tests of the reaction mixture carried out every 10 min during the process using the gas chromatography method. The gas chromatography method provides very high accuracy; however, the reaction mixture was tested 3 times for each time point. The errors calculated on the basis of these measurements are relatively small, and their values are in the range of 2% (the error bars have been plotted on the presented curves). Due to the high conversion achieved, the experiments were carried out for 1 h in all cases. The performed reactions indicated catalytic activity for all examined powders. The substrate



**Figure 8** The Al-13.5 V as-spun ribbon: **a, b** TEM bright-field images, **c-e** SADPs obtained for the separate grains visible in **(a)** with five-, three- and two-fold symmetry of icosahedral quasicrystal, **f, h** SADPs obtained for  $\alpha$ (Al) solid solution taken from the areas between the particles or dendrites shown in **(a, b)** and **g**  $\text{Al}_3\text{V}$  phase obtained for the dendrite in **(b)** taken along [100] zone axis

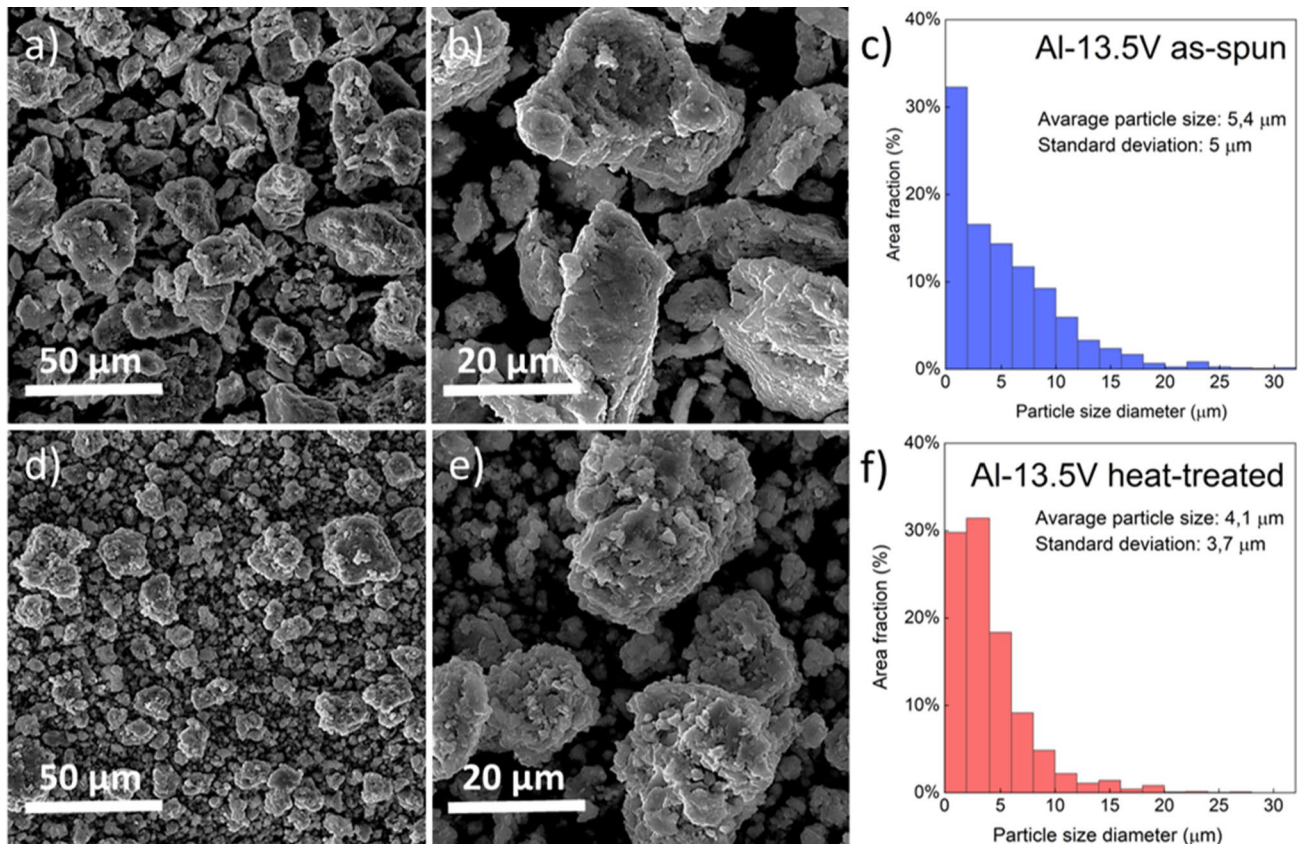
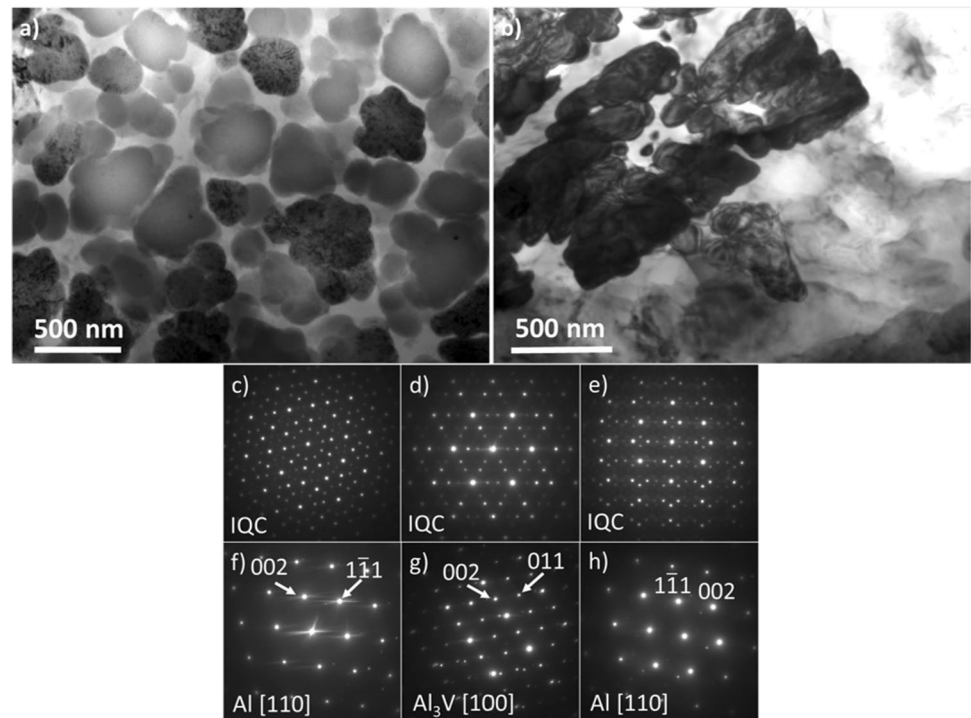


**Figure 9** SEM-BSE micrographs of the Al-13.5 V ribbon after pulverization in the as-spun state **a, b** and annealed powdered ribbon **d, e**, corresponding histograms showing the particle size distribution are seen in **c, f**

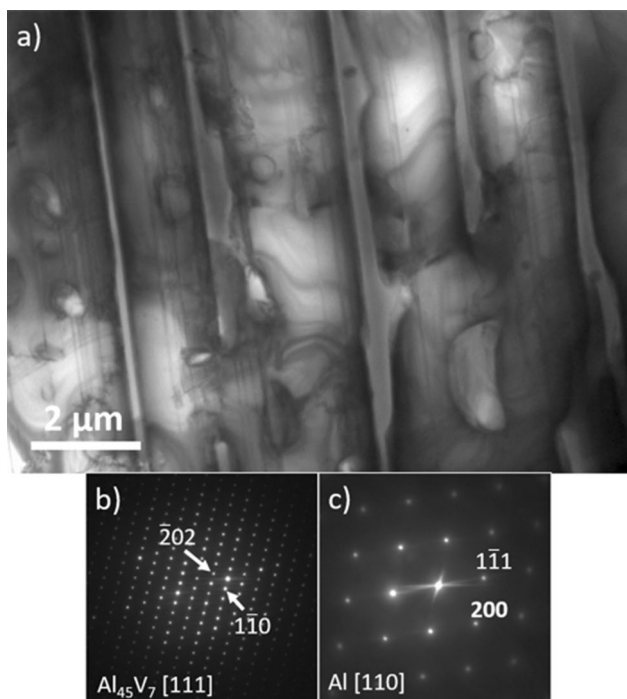
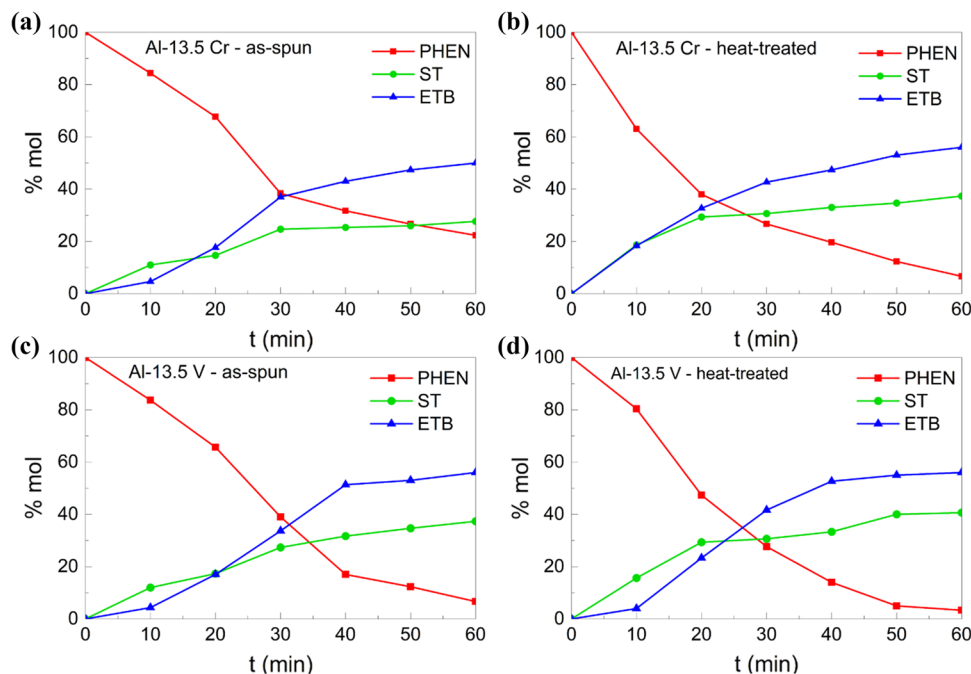


**Figure 10** **a** TEM bright-field image of Al-13.5 V ribbons after annealing for 100 h at 600 °C, SADPs obtained for Al<sub>45</sub>V<sub>7</sub> taken along [111] zone axis **b** and α(Al) solid solution **c**

degree of conversion and selectivity in reactions were determined, and the results are shown in Fig. 11.

For the Al-13.5Cr as-spun powder, the reaction reached a final degree of conversion of 80%, and the activity rate was  $8 \times 10^{-4}$  mol/min  $g_{cat}$  (activity rate expresses the rate of phenylacetylene conversion after 10 min of reaction time per 1 g of applied catalyst). The heat-treated powder provided a degree of conversion of 90% after 1 h, while the activity rate was two times higher and reached the value of  $20.4 \times 10^{-4}$  mol/min  $g_{cat}$ . These results indicate the role of the homogeneity of the catalyst structure on the catalytic properties, as the single-phase Al<sub>45</sub>Cr<sub>7</sub> catalyst provided a higher degree of conversion as well as significantly higher activity. The Al-13.5 V powder in the as-spun state ensured the conversion of the substrate of 90% after 1 h. The heat-treated powder achieved a similar degree of conversion and a slightly higher activity rate of  $11.1 \times 10^{-4}$  mol/min  $g_{cat}$  compared to the powder in as-spun state ( $9 \times 10^{-4}$  mol/min  $g_{cat}$ ). Thus, in the case of the Al-13.5 V ribbon, there was no significant difference in catalyst performance in the as-spun and heat-treated states, despite their various phase compositions. Based on the obtained results, it can be concluded that the activity rates reached similar values for all multiphase alloys tested in this work, unlike the heat-treated single-phase Al-13.5Cr alloy, whose activity was twice as high.

**Figure 11** Hydrogenation of phenylacetylene in the presence of **a** Al-13.5Cr as-spun and **b** Al-13.5Cr heat-treated, **c** Al-13.5 V as-spun and **d** Al-13.5 V heat-treated catalysts. Reaction mixture components were designated: PHEN—phenylacetylene, ST—styrene and ETB—ethylbenzene



These results can be directly compared with those obtained for  $\text{Al}_{71.5}\text{Co}_{28.5}$  and  $\text{Al}_{71.5}\text{Fe}_{28.5}$  catalysts in the form of pulverized melt-spun ribbons thanks to the use of the same reaction conditions [20]. It was found that both groups of materials, shown in this work and previously studied, achieve a similar degree of conversion in the reaction of phenylacetylene hydrogenation. The activity rates after 10 min of reaction also have values of the same order of magnitude. The final styrene content for as-spun Al-13.5Cr and Al-13.5 V alloys was about 30%, which is comparable to the results obtained for as-spun  $\text{Al}_{71.5}\text{Fe}_{28.5}$  alloy. These values were higher than those obtained with the  $\text{Al}_{71.5}\text{Co}_{28.5}$  catalyst under the same conditions. On the other hand, heat-treated Al-13.5Cr and Al-13.5 V alloys allowed to obtain a higher share of styrene, about 40%.

Other experiments of phenylacetylene hydrogenation with transition metal catalysts were performed for Ni-Zn and Ni-Co catalysts on  $\text{SiO}_2$  support with great catalytic performance [34]. The obtained results show the dependence of the set of test conditions on the reaction results. An increase in  $\text{H}_2$  temperature or pressure leads to enhancing the substrate conversion but decreases selectivity to styrene. Since our results showed almost complete phenylacetylene conversion after 1 h, it is worth considering experiments with reduced  $\text{H}_2$  pressure in further study. The same reaction under mild reaction conditions was performed using  $\text{Pd}_2\text{Ga}$  intermetallic powder as a catalyst, which ensured selectivity to styrene in the range of 90% after 4-h reaction time [50]. In addition, a strong influence of reaction conditions and material preparation on the results obtained for this material was indicated. It was also shown that Ni-Ga intermetallic nanoparticles provided high selectivity to styrene in the phenylacetylene hydrogenation reaction [51], but in this case, the reaction time was longer than in the present study. In another study, the properties of nickel-based intermetallic materials prepared by co-impregnation were investigated. Reactions with  $\text{Ni}_3\text{M}/\text{SiO}_2$  ( $\text{M} = \text{Zn}, \text{Sn}, \text{Cd}, \text{Fe}, \text{Co}, \text{Cu}$  or  $\text{Mo}$ ) nanoparticles achieved selectivity in the range of 80–90% with almost complete substrate conversion, but the required reaction time was relatively long, even over 11 h. The next part of the work concerned three-component particles, which provided even better catalytic performance and stability during 6 consecutive reaction cycles [52].

Although the cited studies were performed under different reaction conditions than in our experiment, they indicate the role of material structure on catalytic

performance. It was shown that the tested catalysts had a much better selectivity to styrene compared to the results presented in this work. However, it should be emphasized that the materials we examined have relatively large particle size due to the manufacturing method and tend to be passivated due to the high concentration of Al. Previous experience with aluminium-based catalysts indicates that surface treatment by using  $\text{NaBH}_4$  aqueous solution improves their catalytic properties, but does not eliminate surface oxidation [53]. The melt-spinning method, on the other hand, is not burdensome for the environment, because it does not require the use of precursors for the synthesis reaction, is low-cost, fast and uncomplicated. It also allows the production of large amounts of catalysts without the need to scale the process. The results obtained in this study suggest that the homogeneous Al-13.5Cr and Al-13.5 V intermetallic alloys produced by the melt-spinning can be considered promising catalysts for phenylacetylene hydrogenation reaction, but both the reaction conditions and the catalyst preparation process require further optimization to improve the selectivity to styrene.

## Conclusions

In this work, the catalytic properties of intermetallic compounds from the Al-Cr and Al-V systems were investigated for the first time. The main findings of these studies are as follows:

1. The melt-spinning technique has been used to produce two alloys: Al-13.5 at.% Cr and Al-13.5 at.% V, whose composition corresponded to the quasicrystalline approximants  $\text{Al}_{45}\text{Cr}_7$  and  $\text{Al}_{45}\text{V}_7$ . The as-spun materials had the form of thin (20–70  $\mu\text{m}$ ) brittle ribbons. A part of both alloys was heat-treated for 100 h at 600 °C to homogenize the microstructure.
2. Microstructural studies showed that the as-spun Al-13.5Cr ribbon contained a mixture of  $\text{Al}_{45}\text{Cr}_7$  phase, icosahedral quasicrystal and  $\alpha(\text{Al})$  solid solution. The applied treatment led to the transformation into a single-phase material composed of the stable  $\text{Al}_{45}\text{Cr}_7$  phase.
3. The as-spun Al-13.5 V ribbon consisted of  $\text{Al}_3\text{V}$  phase dendrites and fine spherical particles of icosahedral quasicrystals surrounded by the  $\alpha(\text{Al})$  solid solution. A small amount of  $\alpha(\text{Al})$  solid



solution remained in the annealed ribbon, while the other two phases transformed into the stable  $\text{Al}_{45}\text{V}_7$  phase.

- Catalytic tests were carried out for powdered ribbons (with an average size of about 4  $\mu\text{m}$ ) in the reaction semi-hydrogenation of phenylacetylene to styrene. Experiments conducted under mild conditions ( $\text{H}_2$  pressure of 5 bar in a reactor heated to 50  $^\circ\text{C}$ ) showed catalytic activity with substrate conversion above 80% after 1 h for both, the as-spun and heat-treated powders. Degrees of conversion were slightly higher for the reactions with the heat-treated powder than with the as-spun powder. The highest activity rate,  $20.4 \times 10^{-4} \text{ mol/min g}_{\text{cat}}$ , twice as high as that of the other tested catalysts, was obtained for the heat-treated Al-13.5Cr alloy. Based on the obtained results, it can be concluded that the most promising catalytic performance is related to the homogeneous phase composition and morphology of the material.

The obtained results, which should be treated as preliminary, confirm the potential application of aluminium-based intermetallic alloys produced in the melt-spinning process as catalysts. Therefore, they can become an alternative to currently used catalysts based on noble metals in hydrogenation reactions. However, further research will be needed to optimize all alloy production and reaction steps for the best catalytic performance.

## Acknowledgements

This work was financially supported by the National Science Centre (NCN), Poland, within the project no. 2017/25/B/ST8/02804.

## Author contributions

AZ conceptualization, methodology, investigation, writing—original draft and visualization. KS-G investigation and writing—reviewing and editing. LR resources. PC investigation. JP investigation. RC investigation. DD investigation and resources. LL-D conceptualization, methodology, investigation, writing—original draft, supervision and project administration.

## Declarations

**Conflicts of interest** The authors declare that they have no known competing financial interests or personal relationships that could have appeared to influence the work reported in this paper.

**Open Access** This article is licensed under a Creative Commons Attribution 4.0 International License, which permits use, sharing, adaptation, distribution and reproduction in any medium or format, as long as you give appropriate credit to the original author(s) and the source, provide a link to the Creative Commons licence, and indicate if changes were made. The images or other third party material in this article are included in the article's Creative Commons licence, unless indicated otherwise in a credit line to the material. If material is not included in the article's Creative Commons licence and your intended use is not permitted by statutory regulation or exceeds the permitted use, you will need to obtain permission directly from the copyright holder. To view a copy of this licence, visit <http://creativecommons.org/licenses/by/4.0/>.

## References

- Furukawa S, Komatsu T (2017) Intermetallic compounds, promising inorganic materials for well-structured and electronically modified reaction environments for efficient catalysis. *ACS Catal* 7:735–765. <https://doi.org/10.1021/acscatal.6b02603>
- Marakatti VS, Peter SC (2018) Synthetically tuned electronic and geometrical properties of intermetallic compounds as effective heterogeneous catalysts. *Prog Solid State Chem* 52:1–30. <https://doi.org/10.1016/j.progsolidschem.2018.09.001>
- Dasgupta A, Rioux RM (2019) Intermetallics in catalysis: an exciting subset of multimetallic catalysts. *Catal Today* 330:2–15. <https://doi.org/10.1016/j.cattod.2018.05.048>
- Armbrüster M (2020) Intermetallic compounds in catalysis—a versatile class of materials meets interesting challenges. *Sci Technol Adv Mater* 21:303–322. <https://doi.org/10.1080/14686996.2020.1758544>
- Nakaya Y, Furukawa S (2023) Catalysis of alloys: classification, principles, and design for a variety of materials and reaction. *Chem Rev* 123:5859–5947. <https://doi.org/10.1021/acs.chemrev.2c00356>

- [6] Yang Y, Wei M (2020) Intermetallic compounds catalysts: synthetic scheme, structure characterization and catalytic application. *J Mater Chem A* 8:2207–2221. <https://doi.org/10.1039/C9TA09448B>
- [7] Krajčič M, Hafner J (2016) Intermetallic compounds as selective heterogeneous catalysts: insights from DFT. *ChemCatChem* 8:34–48. <https://doi.org/10.1002/cctc.201500733>
- [8] Gaudry E, Chatelier C, Loffreda D, Kandaskalov D, Coati A, Piccolo L (2020) Catalytic activation of a non-noble intermetallic surface through nanostructuring under hydrogenation conditions revealed by atomistic thermodynamics. *J Mater Chem A* 8:7422–7431. <https://doi.org/10.1039/d0ta01146k>
- [9] Meier M, Ledieu J, Fournée V, Gaudry E (2017) Semihydrogenation of acetylene on Al<sub>5</sub>Co<sub>2</sub> surfaces. *J Phys Chem C* 121:4958–4969. <https://doi.org/10.1021/acs.jpcc.6b11083>
- [10] Tsai AP, Kameoka S, Nozawa K, Shimodan M, Ishii Y (2017) Intermetallic: a pseudoelement for catalysis. *Acc Chem Res* 50:2879–2885. <https://doi.org/10.1021/acs.accounts.7b00476>
- [11] Ledieu J, Gaudry E, Fournée V (2014) Surfaces of Al-based complex metallic alloys: atomic structure, thin film growth and reactivity. *Sci Technol Adv Mater* 15:034802. <https://doi.org/10.1088/1468-6996/15/3/034802>
- [12] Armbrüster M, Schlögl R, Grin Y (2014) Intermetallic compounds in heterogeneous catalysis—a quickly developing field. *Sci Technol Adv Mater* 15:034803. <https://doi.org/10.1088/1468-6996/15/3/034803>
- [13] Piccolo L, Kibis L, De Weerd MC (2017) Intermetallic compounds as potential alternatives to noble metals in heterogeneous catalysis: the partial hydrogenation of butadiene on  $\gamma$ -Al<sub>4</sub>Cu<sub>9</sub> (110). *ChemCatChem* 9:2292–2296. <https://doi.org/10.1002/cctc.201601587>
- [14] Chen X, Ma Y, Wang L, Yang Z, Jin S, Zhang L, Liang C (2015) Nickel-Aluminum intermetallic compounds as highly selective and stable catalysts for the hydrogenation of naphthalene to tetralin. *ChemCatChem* 7:978–983. <https://doi.org/10.1002/cctc.201402957>
- [15] Kameoka S, Tanabe T, Satoh F, Terauchi M, Tsai AP (2014) Activation of Al–Cu–Fe quasicrystalline surface: fabrication of a fine nanocomposite layer with high catalytic performance. *Sci Technol Adv Mater* 15:014801. <https://doi.org/10.1088/1468-6996/15/1/014801>
- [16] Czaja P, Boochani A, Przewoźnik J, Yeganeh JM, Zelati A, Yari A, Amiri M, Naderi S, Fitta M, Duraczyńska D, Serwicka EM, Stan-Głowińska K, Lityńska-Dobrzyńska L (2022) Microstructure, catalytic activity, magnetic and electronic properties of Ni<sub>3</sub>Al, Ni<sub>3</sub>Ga and Ni<sub>3</sub>Sn melt spun intermetallics from experimental and DFT computational standpoints. *J Alloys Compd* 927:167076. <https://doi.org/10.1016/j.jallcom.2022.167076>
- [17] Armbrüster M, Kovnir K, Friedrich M, Teschner D, Wownick G, Hahne M, Gille P, Szentmiklósi L, Feuerbacher M, Heggen M, Girgsdies F, Rosenthal D, Schlögl R, Grin Yu (2012) Al<sub>13</sub>Fe<sub>4</sub> as a low-cost alternative for palladium in heterogeneous hydrogenation. *Nat Mater* 11:690–693. <https://doi.org/10.1038/NMAT3347>
- [18] Piccolo L, Chatelier C, de Weerd MC, Morfin F, Ledieu J, Fournée V, Gille P, Gaudry E (2019) Catalytic properties of Al<sub>13</sub>TM<sub>4</sub> complex intermetallics: influence of the transition metal and the surface orientation on butadiene hydrogenation. *Sci Technol Adv Mater* 20:557–567. <https://doi.org/10.1080/14686996.2019.1608792>
- [19] Zięba A, Stan-Głowińska K, Czaja P, Rogal Ł, Przewoźnik J, Duraczyńska D, Serwicka EM, Lityńska-Dobrzyńska L (2022) Microstructure and catalytic activity of Al<sub>13</sub>Fe<sub>4</sub> and Al<sub>13</sub>Co<sub>4</sub> melt-spun alloys. *Microsc Microanal* 28:961–967. <https://doi.org/10.1017/S1431927621012320>
- [20] Zięba A, Stan-Głowińska K, Rogal Ł, Cios G, Czaja P, Przewoźnik J, Chulist R, Duraczyńska D, Serwicka EM, Lityńska-Dobrzyńska L (2022) Microstructure and catalytic properties of rapidly solidified Al-28.5 at% Fe and Al-28.5 at% Co alloys applied for selective hydrogenation of phenylacetylene. *Mater Today Commun* 33:104422. <https://doi.org/10.1016/j.mtcomm.2022.104422>
- [21] Chatelier C, Garreau Y, Piccolo L, Vlad A, Resta A, Ledieu J, Fournée V, De Weerd MC, Picca FE, De Boissieu M, Felici R, Coati A, Gaudry É (2020) From the surface structure to catalytic properties of Al<sub>5</sub>Co<sub>2</sub> (21 $\bar{1}$ 0): a study combining experimental and theoretical approaches. *J Phys Chem C* 124:4552–4562. <https://doi.org/10.1021/acs.jpcc.9b09675>
- [22] Han B, Ma P, Cong X, Chen H, Zeng X (2019) Chromium- and cobalt-catalyzed, regiocontrolled hydrogenation of polycyclic aromatic hydrocarbons: a combined experimental and theoretical study. *J Am Chem Soc* 141:9018–9026. <https://doi.org/10.1021/jacs.9b03328>
- [23] Hirscher NA, Sierra DP, Agapie T (2019) Robust chromium precursors for catalysis: isolation and structure of a single-component ethylene tetramerization precatalyst. *J Am Chem Soc* 141:6022–6029. <https://doi.org/10.1021/jacs.9b01387>
- [24] Gregori BJ, Nowakowski M, Schoch A, Pöllath S, Zweck J, Bauer M, Jacobi von Wangelin A (2020) Stereoselective chromium-catalyzed semi-hydrogenation of alkynes. *ChemCatChem* 12:5359–5363. <https://doi.org/10.1002/cctc.202000994>
- [25] Langeslay RR, Kaphan DM, Marshall CL, Stair PC, Sattelberger AP, Delferro M (2019) catalytic applications of

- vanadium: a mechanistic perspective. *Chem Rev* 119:2128–2191. <https://doi.org/10.1021/acs.chemrev.8b00245>
- [26] Okamoto H (2008) Al-Cr (Aluminum-chromium). *J Phase Equilib Diffus* 29:112–113. <https://doi.org/10.1007/s11669-007-9225-4>
- [27] He ZB, Zou BS, Kuo KH (2006) The monoclinic Al<sub>45</sub>Cr<sub>7</sub> revisited. *J Alloys Compd* 417:9–13. <https://doi.org/10.1016/j.jallcom.2005.09.034>
- [28] Brix AF, Simon R, Gaudry E (2020) The (010) surface of the Al<sub>45</sub>Cr<sub>7</sub> complex intermetallic compound: insights from density functional theory. *Z Anorg Allg Chem* 646:1176–1182. <https://doi.org/10.1002/zaac.202000081>
- [29] Zhang H, Wang DH, Kuo KH (1988) Quasicrystals, crystal-line phases, and multiple twins in rapidly solidified Al-Cr alloys. *Phys Rev B* 37:6220–6225
- [30] Okamoto H (2012) Al-V (Aluminum-vanadium). *J Phase Equilib Diffus* 33:491. <https://doi.org/10.1007/s11669-012-0090-4>
- [31] Brown PJ (1959) The Structure of the intermetallic phase  $\alpha'$  (VAl). *Acta Crystallogr A* 12:995–1002
- [32] Lawther DW, Lloyd DJ, Dunlap RA (1990) Transition metal site distributions in binary aluminum-transition metal quasicrystals: AlV and AlCr. *Mater Sci Eng A* 123:33–38. [https://doi.org/10.1016/0921-5093\(90\)90206-1](https://doi.org/10.1016/0921-5093(90)90206-1)
- [33] Grushko B, Velikanova TY (2004) Stable and metastable quasicrystals in Al-based alloy systems with transition met-als. *J Alloys Compd* 367:58–63. <https://doi.org/10.1016/j.jallcom.2003.08.012>
- [34] Chen W, Bao Z, Zhou Z (2022) Selective hydrogenation of phenylacetylene over non-precious bimetallic Ni–Zn/SiO<sub>2</sub> and Ni–Co/SiO<sub>2</sub> catalysts prepared by glucose pyrolysis Reaction Kinetics. *Mech Catal* 135:2533–2550. <https://doi.org/10.1007/s11144-022-02276-w>
- [35] Rodriguez-Carvajal J (1993) Recent advances in mag-netic structure determination by neutron powder diffrac-tion. *Physica B* 192:55–69. [https://doi.org/10.1016/0921-4526\(93\)90108-1](https://doi.org/10.1016/0921-4526(93)90108-1)
- [36] Wojcik A, Chulist R, Czaja P, Kowalczyk M, Zackiewicz P, Schell N, Maziarz W (2021) Evolution of microstructure and crystallographic texture of Ni-Mn-Ga melt-spun rib-bons exhibiting 11.5% magnetic field-induced strain. *Acta Mater* 219:117237. <https://doi.org/10.1016/j.actamat.2021.117237>
- [37] Zupanič F, Bončina T, Šuštaršič B, Anžel I, Markoli B (2008) Microstructure of Al–Mn–Be melt-spun ribbons. *Mater Charact* 59:1245–1251. <https://doi.org/10.1016/j.matchar.2007.10.007>
- [38] Stan K, Lityńska-Dobrzyńska L, Ochín P, Wierzbička-Miernik A, Góral A, Wojewoda-Budka J (2013) Effect of alloying elements on microstructure and properties of Al-Mn-Fe ribbon. *Arch Metall Mater* 58:341–346. <https://doi.org/10.2478/v10172-012-0195-0>
- [39] Kang HJ, Hu ZL, Gao XX, Chen ZN, Lu YP, Jie JC, Guo JJ (2016) 3D Morphology and Formation Process of the Ico-sahedral Quasicrystalline Phase in Rapidly Solidified Al–Mn Alloy. *Acta Metall Sin (Engl Lett)* 29:28–31. <https://doi.org/10.1007/s40195-015-0357-y>
- [40] Boulet P, de Weerd MC, Gaudry E, Ledieu J, Fournée V (2020) Single crystal growth, crystal structure and surface characterization of the binary phase Al<sub>45</sub>Cr<sub>7</sub>. *J Phys Conf Ser* 1458:012016. <https://doi.org/10.1088/1742-6596/1458/1/012016>
- [41] Lawther DW, Dunlap RA, Srinivas V (1989) On the ques-tion of stability and disorder in icosahedral aluminum–tran-sition metal alloys. *Can J Phys* 67:467:463–467. <https://doi.org/10.1139/p89-082>
- [42] Inoue A, Kimura H, Masumoto T (1987) Formation, thermal stability and electrical resistivity of quasicrystal-line phase in rapidly quenched Al-Cr alloys. *J Mater Sci* 22:1758–1768. <https://doi.org/10.1007/BF01132404>
- [43] Swamy VT, Ranganathan S, Chattopadhyay K (1989) Rap- idly solidified Al-Cr alloys: Crystalline and quasicrystalline phases. *J Mater Res* 4:539–551. <https://doi.org/10.1557/JMR.1989.0539>
- [44] Kobayashi KF, Tachibana N, Shingu PH (1989) Continuous heating of rapidly solidified Al-Cr ribbons. *J Mater Science* 24:2437–2443. <https://doi.org/10.1007/BF01174508>
- [45] Rosen GI, Shechtman D (1994) Formation of microstruc-ture of the icosahedral phase in rapidly solidified alumin-ium-chromium alloys. *Acta metall mater* 42:177–184. [https://doi.org/10.1016/0956-7151\(94\)90060-4](https://doi.org/10.1016/0956-7151(94)90060-4)
- [46] Czaja P, Chulist R, Wójcik A, Kowalczyk M, Zackiewicz P, Szewczyk A, Schell N, Maziarz W (2021) Suppression and recovery of martensitic transformation and magnet-ism in mechanically and thermally treated magnetic shape-memory Ni–Mn–Ga melt-spun ribbons. *Adv Eng Mater* 23:2100075. <https://doi.org/10.1002/adem.202100075>
- [47] Maziarz W, Czaja P, Chulist R, Wójcik A, Żrodowski Ł, Morończyk B, Wróblewski R, Kowalczyk M (2021) Micro-structure and magnetic properties of selected laser melted ni-mn-ga and ni-mn-ga-fe powders derived from as melt-spun ribbons precursors. *Metals* 11:903. <https://doi.org/10.3390/met11060903>
- [48] Maas J, Bastin G, van Loo F, Metselaar R (1983) The texture in diffusion-grown layers of Trialuminides MeAl<sub>3</sub>(Me=Ti, V, Ta, Nb, Zr, Hf) and VN<sub>3</sub>. *Intern J Mater Res* 74:294–299. <https://doi.org/10.1515/ijmr-1983-740506>
- [49] Inoue A, Arnberg L, Lehtinen B, Oguchi M, Masumoto T (1986) Compositional analysis of the icosahedral phase in rapidly quenched Al-Mn and Al-V alloys. *Metall Mater*



- Trans A 17:1657–1664. <https://doi.org/10.1007/BF02817264>
- [50] Wowsnick G, Teschner D, Armbrüster M, Kasatkin I, Girgsdies F, Grin Y, Schlögl R, Behrens M (2014) Surface dynamics of the intermetallic catalyst Pd<sub>2</sub>Ga, Part II - Reactivity and stability in liquid-phase hydrogenation of phenylacetylene. *J Catal* 309:221–230. <https://doi.org/10.1016/j.jcat.2013.09.018>
- [51] Li C, Chen Y, Zhang S, Zhou J, Wang F, He S, Wei M, Evans DG, Duan X (2014) Nickel-gallium intermetallic nanocrystal catalysts in the semihydrogenation of phenylacetylene. *Chem Cat Chem* 6:824–831. <https://doi.org/10.1002/cctc.201300813>
- [52] Chen W, Xu H, Ma X, Qi L, Zhou Z (2023) Synergistic trimetallic Ni–Cu–Sn catalysts for efficient selective hydrogenation of phenylacetylene. *Chem Eng J* 455:140565. <https://doi.org/10.1016/j.cej.2022.140565>
- [53] Lityńska-Dobrzyńska L, Stan-Głowińska K, Wójcik A, Duraczyńska D, Serwicka EM (2020) Microstructure and catalytic activity of melt spun Al-Cu-Fe Ribbons. *Mater Sci Forum* 985:109–114

**Publisher's Note** Springer Nature remains neutral with regard to jurisdictional claims in published maps and institutional affiliations.